iJRASET
International Journal For Research in Applied Science and Engineering Technology

INTERNATIONAL JOURNAL FOR RESEARCH

IN APPLIED SCIENCE & ENGINEERING TECHNOLOGY

Volume: 6 **Issue:** XII **Month of publication:** December 2018

DOI:

www.ijraset.com

Call: 08813907089 | E-mail ID: ijraset@gmail.com

International Journal for Research in Applied Science & Engineering Technology (IJRASET)
ISSN: 2321-9653; IC Value: 45.98; SJ Impact Factor: 6.887
Volume 6 Issue XII, Dec 2018- Available at www.ijraset.com

Synthesis and Characterization of $LiMn_2O_4$ Nanocomposite Electrode Material for Renewable Energy Storage

Subhashini.Vedala[1], M. Sushama[2]
[1, 2]*EEE Department, Jntuhceh, JNTU, Hyderabad 500085, India.*

Abstract: ***This paper explains the synthesis of most interesting $LiMn_2O_4$ Nanocomposite Electrode Material as a cathode, calcinated at different temperatures for lithium ion secondary batteries, synthesized by a facile co-precipitation method and characterized by different techniques such as X-Ray Diffraction for crystalinity and crystal phase information and its indicates that the sintering temperature affects the formation of spinel phase, and prominent $LiMn_2O_4$ spinel powder with smaller atom location confusion forms about 800°C morphology & elemental composition by Scanning electron microscopy (SEM) with EDAX analysis, FTIR spectroscopy for structure elucidation, & TG–DTA shows that the weight loss occurs in four temperature regions during the synthesis of $LiMn_2O_4$.***

Keywords: X-Ray Diffraction, Scanning electron microscopy (SEM), FTIR spectroscopy, TG–DTA .

I. INTRODUCTION

This Lithium-ion batteries have become the most important storage technology in the field of portable, mobile applications (such as laptops, mobile phones) within a few years. In relation to lead or NiCd batteries, very high gravimetric energy densities of more than 150 Wh / kg provide a decisive competitive advantage in this market segment, so that the still high specific costs can be enforced. In discussing lithium battery technologies, it should be noted that this is not a uniform concept, such as the use of lithium battery technology. can be assumed with lead and NiCdBatterien. Due to the large number of possible material combinations, there are still high development efforts and it is still unclear which of the concepts have the best properties for use in the field of large storage systems, as they are necessary in the network or in the electric traction field, will have. In particular, it is still unclear how far the cycle life can be increased. This parameter is critical to the overall economics of storage systems. The power densities achieved today of up to 2,500 W / kg (which was considered impossible just a few years ago) are already sufficient for most conceivable applications. The high cell voltage of up to 3.6 V / cell facilitates the construction of high-voltage storage systems. However, it is necessary to protect each individual cell with safety and protection electronics. Due to the high activity of lithium metal and the high energy density, safe operation is only guaranteed if the operating voltage window is maintained very precisely. Since individualizing cells in series circuits, the monitoring of the total string is not enough. Still high costs in the range of 500 to 1000 € / kWh and questions of safety are still in the way of a broad introduction in stationary and automotive applications. However, it can be expected that lithium battery technology, along with lead battery technology, will become the primary battery technology for at least the next 20 years. A significant increase in energy density compared to today's level can only be expected by switching to fuel cell technologies. However, these are characterized by a much more complex system technology and it remains to be seen which technology will be in the lead here. Predominantly price and service life play the decisive role for stationary applications.

II. SYNTHESIS

Nano scale pure phase LiMn2O4 composite material is synthesized by low temperature method from Metal chloride salts . As many properties are dependent on the size and morphology this method helped to achieve the desired results.Stoichiometric mixture of lithium chloride LiCl (MERCH INDIA) and manganese chloride MnCl2 were separately dissolved in double distilled water at a predetermined molar ratio of Li:Mn , as 0:2 and mixed drop wise , when precursor solution get stabilizes, stoichiometric ratio of sodium is added under vigorous stirring. Stirring and heating of the reaction mixture is continued after addition of hydroxide solution to form aqueous metal solution. Sodium hydroxide solution is added and it acts as reducing agent. The solution containing active material was constantly stirred at 80^0C for 6 hours .The excess of water was removed by Ultrasonic irradiation stirring in a mini ultrasonicator (50W, 28 kHz) after filtering, the active material were washed with deionized water and dried at 110^0C for 12 hours. The $LiMn_2O_4$ powder obtained were heat treated at 700^0C for 5 hours at ambient condition and then air cooled to room

temperature yielding dark powder. The particle size, appearance, phase composition of obtained $LiMn_2O_4$ depend on type of solvent, the reaction temperature and stirring conditions. Schematic diagram of experiment is shown in figure.

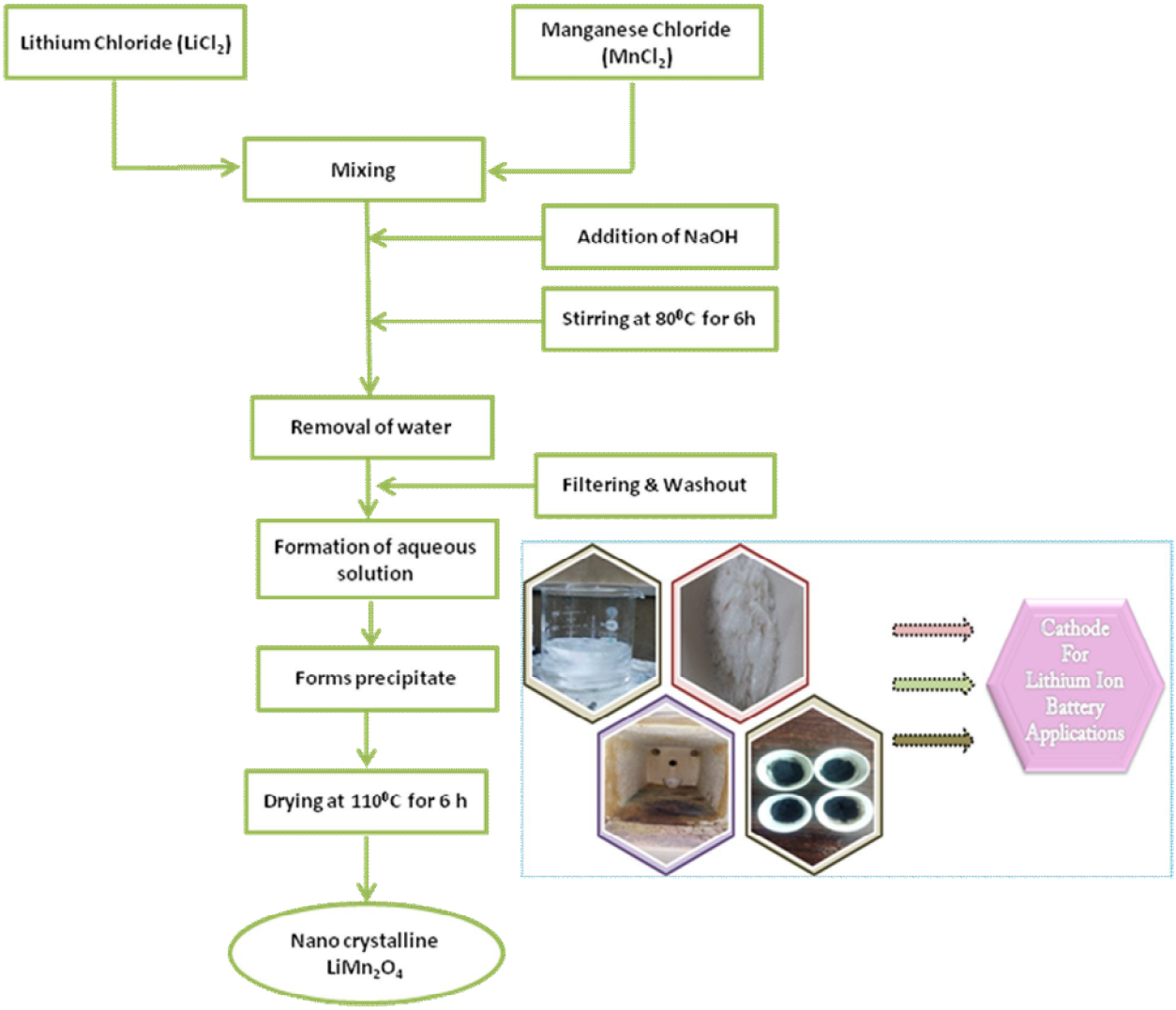

Fig. 1 Flow chart for the preparation of $LiMn_2O_4$ cathode

III.RESULTS AND DISCUSSION

A. XRD Characterization

Crystallography structure and crystallite size of synthesized nano $LiMn_2O_4$ powders determined by X-ray diffraction (XRD, Bruker D& Advance, Germany) using CuKα as radiation source (40kv, step size 0.02°, scan rate 0.5° min^{-1}, $10° \leq 2\theta \leq 80°$) Fig. shows the XRD pattern of the synthesized $LiMn_2O_4$ nano powders. All samples are in conformity of the JCPDS card no 35-0782, and diffraction peaks are corresponding to the cubic spinel structure with Fd3m space group. The peaks are observed at 2θ around 18.66, 36.23, 38.23, 44.31, 48.4, 58.3, 64.49 degree is related to the plans [1 1 1], [3 1 1], [4 0 0], [5 1 1], [4 4 0] respectively. In this space group Li+ fills lattice sites on the tetrahedral 8a, Mn^{3+}, Mn^{4+} are located on the octahedral 16d and O^{2-} on the 32e [63].

XRD results indicate that the product obtained is single phase spinel structure with minor impure phases. X-ray diffraction (XRD) pattern is an efficient method for determining the different phases present in the sample. Since the wavelength of X-rays used is of the same order of magnitude as the interatomic distances and bond lengths in crystalline solids (~1 Å), the XRD method serves well to determine the structure of crystalline materials. The cubic structure of the $LiMn_2O_4$ nanomaterials are studied in this thesis facilitates the determination of the lattice parameter 'a' from one diffraction peak according to:

$$\frac{1}{d} = \frac{\sqrt{h2 + k2 + l2}}{a} \qquad \text{---------- (1)}$$

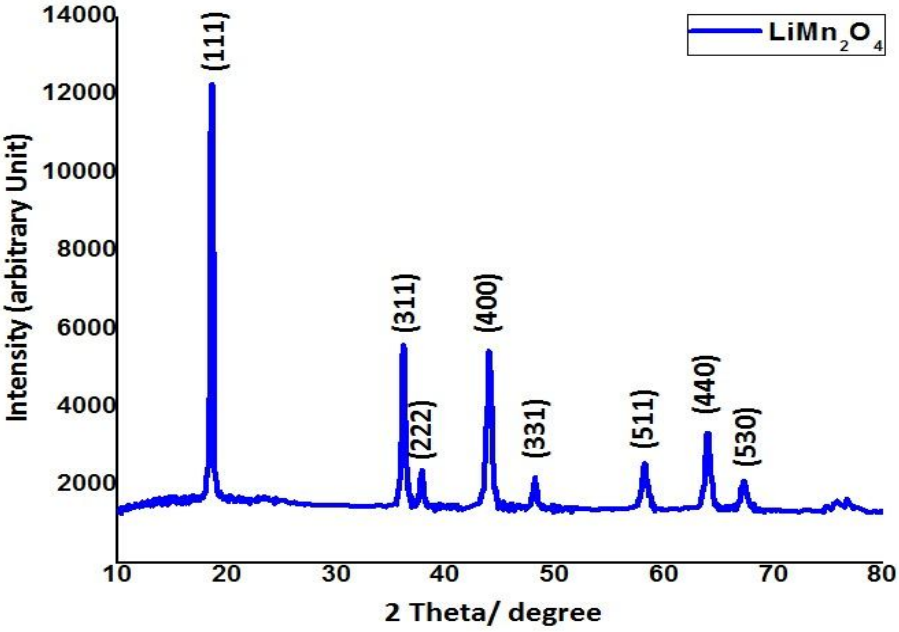

Fig. 2 X-ray diffraction pattern of nanocrystalline $LiMn_2O_4$

Where d is the spacing of the crystal planes and h, k, l are the Miller indices of the measured reflection. Average lattice parameter' a'=0.8198nm=8.198 A°. The study of ion-insertion processes in electrode materials has been shown to be particularly amenable to in situ X-ray diffraction (XRD) methodology. Its advantage lies in its ability to monitor structural changes in the electrode material as ion insertion or de-insertion process.

The average crystal size of the samples was calculated using Debye Scherer's formula

$$D = \frac{0.9\lambda}{\beta cos\theta}$$

Average crystal size=26.59nm

Constructive interference of X-ray radiation occurs in a material when Bragg's law is satisfied

$$2d\ sin\theta = n\lambda$$

Where d is the distance between equivalent atomic planes, Θ is the angle between the incident beam and these planes(Bragg angle), n is an integer and λ is wavelength of X-ray beam ($Cu_{k\alpha}$=1.5406),d spacing of lattice planes depends on the size of the unit cell and determines the position of the peaks. The domain size became quite small, indicating the low lattice strain when the sample is heat treated at 700°C

Stoke's strain values are calculated using the following formula

$$\text{Strain} \quad \varepsilon = \frac{\beta cos\theta}{4Sin\theta}$$

And its value at major peak is 0.00366.

The line width and shape of the peaks derived from conditions of measuring particle size of the sample material. Li insertion/de-insertion and size depends up on synthesis methods. Average values of crystal size, lattice parameter, volume and strain are listed below:

1) Crystal size=29.28nm
2) Lattice parameter=0.8163nm=8.16 A°
3) Volume = 549.35$A^{\circ 3}$
4) Strain =0.002877

Generally, the electrochemical performances of electrode materials are sturdily influenced by the phase crystallinity, particle size, purity and distribution. These factors depend upon synthesis methods.

B. Thermo Gravimetric Analysis (TGA) and Differential thermal analysis (DTA)

In the present work thermal decomposition behavior of the precursors were investigated by thermo gravimetric analysis and differential thermal analysis (TG- DTA, A6300R) in the temperature range of 0-800^{o}C for inorganic-organic polymer hybrid materials using alumina crucibles with 20 mg of Al samples, under air with a heating rate at 20^{o}C min-1.

The thermal decomposition behavior of $LiMn_2O_4$ were investigated by thermo gravimetric analysis. Fig.5.3 (a) and (b) shows the thermal gravimetric analysis (TGA) curves of $LiMn_2O_4$ nano powders. Generally weight loss of the sample occurred at two stages which are called as stage corresponded to temperature between 25 – 125 °C, 325 – 800 °C, respectively. Weight loss at these temperatures represents exothermic reaction(emit energy) and weight gain at a temperature range of 125°C -225°C represents endothermic reaction (emit energy). For all temperature ranges sample exhibits low weight loss which are less than 1% have occurred that are charge to the oxygen loss. However, it should be mentioned these temperatures ranges are not fixed anywhere and in each case they can be changed, but these ranges are mainly and common in all samples.

From figure 5.3 it seems the entire samples have most decomposition low weight lost was observed because of carbon decomposition. However the temperature ranges of the decompositions are different. DTA graphs have shown only exothermic peaks, all the endothermic peaks were belong to the water evaporated. These lower weight loss of TG/DTA graphs represents nano $LiMn_2O_4$ cathode material is thermally stable.

C. Sem Analysis

Particle Morphology of Nano $LiMn_2O_4$ was examined through SEM and TEM Images. To measure the physical grain size of the spinel product, the SEM analysis was made out on sample annealed at 700 °C. The SEM images of synthesized nanopowder of $LiMn_2O_4$ by nano materials showed smaller morphology with similar particle shape in micro meter and nano meter scale of 200nm.Average grain size being lower than 2μm and nearly pore Free State is evidence from the micrograph. The grains are almost connected and ensured the high surface area. The above-mentioned features are very desirable for an electrode material to be used as a cathode – active material for the modern high energy Li-ion rechargeable batteries.

IV. CONCLUSIONS

The electro active spinel $LiMn_2O_4$ has been synthesized by sol-gel method. Power X-ray diffraction analysis shows that the sample has pure single phase and good crystallinity with average size 31 nm , moropology examined by FESEM shows that LiMn2o4 composite material exhibits homogeneous particle distribution to gain high specific capacity and good cyclability for Lithium ion batteries applicable for renewable energy storage applications.

REFERENCES

[1] S. M. Metev and V. P. Veiko, Laser Assisted Microtechnology, 2nd ed., R. M. Osgood, Jr., Ed. Berlin, Germany: Springer-Verlag, 1998.
[2] J. Breckling, Ed., The Analysis of Directional Time Series: Applications to Wind Speed and Direction, ser. Lecture Notes in Statistics. Berlin, Germany: Springer, 1989, vol. 61.
[3] S. Zhang, C. Zhu, J. K. O. Sin, and P. K. T. Mok, “A novel ultrathin elevated channel low-temperature poly-Si TFT,” IEEE Electron Device Lett., vol. 20, pp. 569–571, Nov. 1999.
[4] M. Wegmuller, J. P. von der Weid, P. Oberson, and N. Gisin, “High resolution fiber distributed measurements with coherent OFDR,” in Proc. ECOC’00, 2000, paper 11.3.4, p. 109.
[5] R. E. Sorace, V. S. Reinhardt, and S. A. Vaughn, “High-speed digital-to-RF converter,” U.S. Patent 5 668 842, Sept. 16, 1997.
[6] (2002) The IEEE website. [Online]. Available: http://www.ieee.org/
[7] M. Shell. (2002) IEEEtran homepage on CTAN. [Online]. Available: http://www.ctan.org/tex-archive/macros/latex/contrib/supported/IEEEtran/
[8] FLEXChip Signal Processor (MC68175/D), Motorola, 1996.
[9] “PDCA12-70 data sheet,” Opto Speed SA, Mezzovico, Switzerland.
[10] A. Karnik, “Performance of TCP congestion control with rate feedback: TCP/ABR and rate adaptive TCP/IP,” M. Eng. thesis, Indian Institute of Science, Bangalore, India, Jan. 1999.
[11] J. Padhye, V. Firoiu, and D. Towsley, “A stochastic model of TCP Reno congestion avoidance and control,” Univ. of Massachusetts, Amherst, MA, CMPSCI Tech. Rep. 99-02, 1999.
[12] Wireless LAN Medium Access Control (MAC) and Physical Layer (PHY) Specification, IEEE Std. 802.11, 1997.

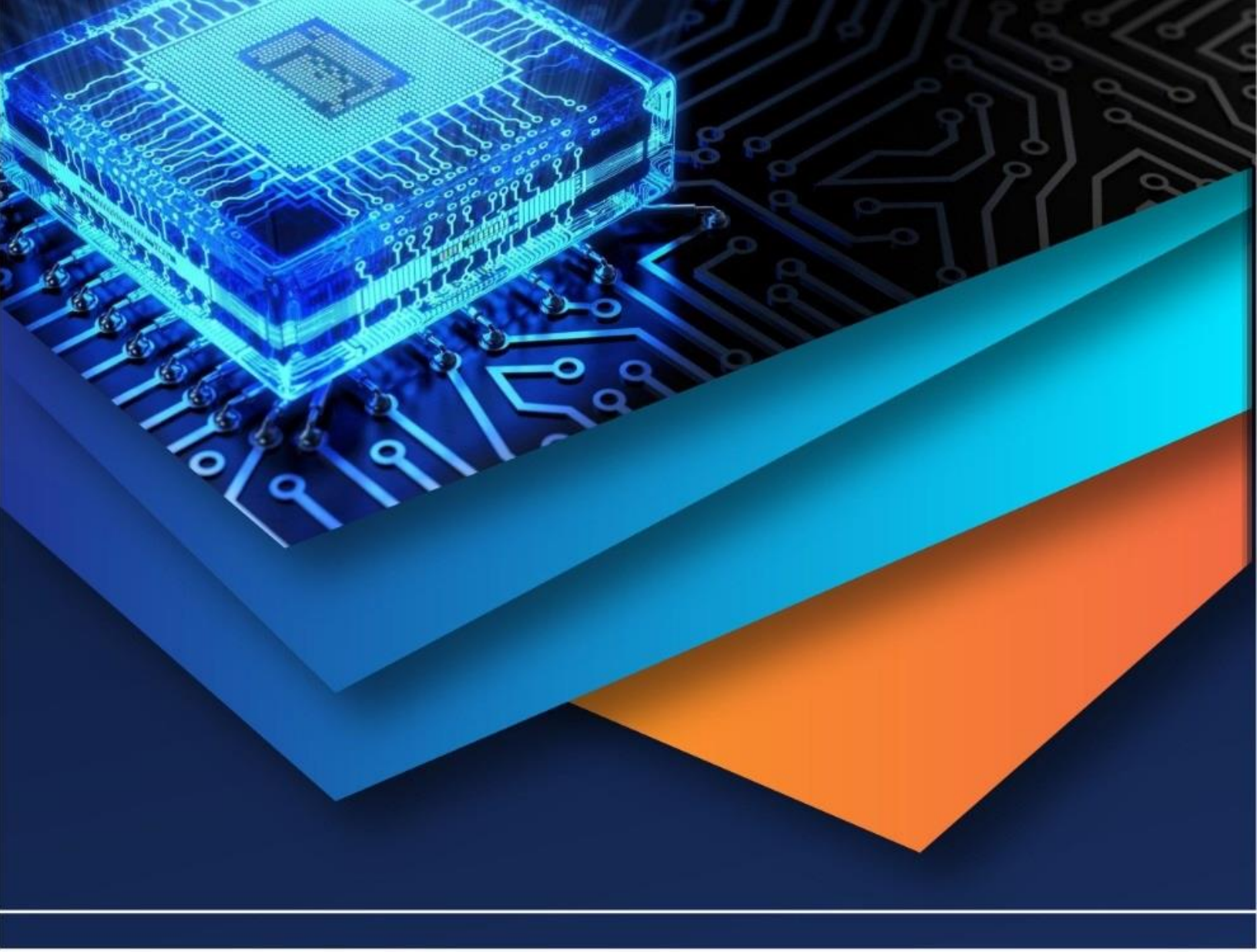

10.22214/IJRASET

45.98

IMPACT FACTOR: 7.129

IMPACT FACTOR: 7.429

INTERNATIONAL JOURNAL FOR RESEARCH

IN APPLIED SCIENCE & ENGINEERING TECHNOLOGY